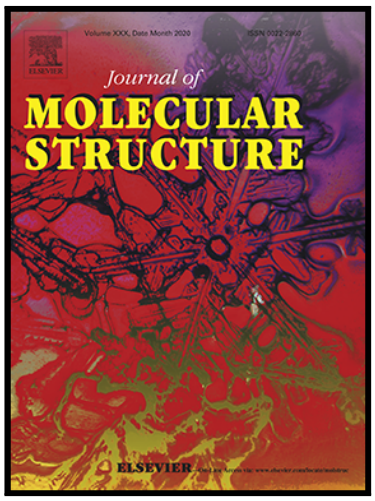

X-Ray structure, Hirshfeld analysis and DFT studies of two new hits of triazolyl-indole bearing alkylsulfanyl moieties

Ahmed T.A. Boraei , Saied M. Soliman , Matti Haukka , Assem Barakat

PII: S0022-2860(20)31622-7
DOI: https://doi.org/10.1016/j.molstruc.2020.129302
Reference: MOLSTR 129302

To appear in: *Journal of Molecular Structure*

Received date: 29 June 2020
Revised date: 8 August 2020
Accepted date: 17 September 2020

Please cite this article as: Ahmed T.A. Boraei , Saied M. Soliman , Matti Haukka , Assem Barakat , X-Ray structure, Hirshfeld analysis and DFT studies of two new hits of triazolyl-indole bearing alkylsulfanyl moieties, *Journal of Molecular Structure* (2020), doi: https://doi.org/10.1016/j.molstruc.2020.129302

Highlights

- Synthesis of two new hits based triazolyl-indole bearing alkylsulfanyl moieties.
- The molecular structure assigned by single crystal X-ray diffraction technique.
- Molecular insights including Hirshfeld analysis, DFT, and their reactivity descriptors were investigated.
- The NBO, Uv-Vis and NMR spectra were also discussed.

X-Ray structure, Hirshfeld analysis and DFT studies of two new hits of triazolyl-indole bearing alkylsulfanyl moieties

Ahmed T. A. Boraei[1,*], Saied M. Soliman[2], Matti Haukka[3], and Assem Barakat[4*]

1 Chemistry Department, Faculty of Science, Suez Canal University, Ismailia 41522, Egypt

2 Department of Chemistry, Faculty of Science, Alexandria University, P.O. Box 426, Ibrahimia, Alexandria 21321, Egypt.

3 Department of Chemistry, University of Jyväskylä, P.O. Box 35, FI-40014 Jyväskylä, Finland

4 Department of Chemistry, College of Science, King Saud University, P.O. Box 2455, Riyadh 11451, Saudi Arabia

***** Correspondence: ahmed_tawfeek83@yahoo.com (A.T.A.B.); Assem Barakat: ambarakat@ksu.edu.sa

Abstract

Two new hits of triazolyl-indole containing two different alkylsulfanyl analogues named *tert*-butyl 2-((4-amino-5-(1*H*-indol-2-yl)-4*H*-1,2,4-triazol-3-yl)thio)acetate **2**, and ethyl 2-((4-amino-5-(1*H*-indol-2-yl)-4*H*-1,2,4-triazol-3-yl)thio)acetate **3** were synthesized *via* reaction of 4-amino-5-(1*H*-indol-2-yl)-1,2,4-triazol-3(2*H*)-thione **1** with *tert*-butyl bromoacetate and ethyl chloroacetate in the presence of base (Et_3N). The molecular structure of **2**, and **3** was confirmed by single-crystal X-ray diffraction and $^{1}H/^{13}C$- NMR spectroscopic techniques. In compound **2**, the molecular packing depends on significant O...H (9.3%), N...H (12.4%) and S...H (3.1%) as well as relatively weak C...H (14.1%), S...C (2.1%), H...H (50.5%) and S...S (0.9%) contacts. Similarly, the strong O...H (11.0-12.3%) and N...H (13.1-13.6%) hydrogen bonds as well as weak C...H (15.3-16.4%), S...N (0.8-1.7%) and H...H (43.6-43.9%) are the most important interactions compound in **3**. Both compounds are polar molecules where hit **2** (0.980 Debye) is less polar than **3** analogue (5.029 Debye). The atomic charge distribution

and molecular electrostatic potential map as well as the reactivity descriptors were also discussed. The calculated NMR and UV-Vis spectra of the studied compounds were computed and compared with the experimental data. The different σ→σ*, π→π*, n→σ* and n→π* donor-acceptor interactions were investigated using NBO analysis.

Keywords: triazolyl-indole; Hirshfeld surface analysis; DFT; reactivity descriptors; NBO; Uv-Vis.

Introduction

The synthesis of new material science and their applications incorporating triazolyl-indole scaffold have received extensive attention over the years with the aim of discovery of new synthetic leads [1-11]. For instance, a series of triazolyl-indole integrated with sulfide moiety was synthesized and screened *in vitro* for anti-cancer activities against different cancer cell lines (MDA-MB-231, HeLa, and KG1a) by Westwell, A.D. group [12,13]. The authors revealed that nitro substituted group of triazolyl-indole scaffold exhibited high efficacy as anti-cancer potential which expressed Bc1-2- human cancer cell lines in the BH3 binding pocket[12,13].

Moreover, a new series of triazolyl-indole containing sulfanyl moiety were reported and assessed *in vitro* for inhibitory activities against anti-proliferative activity [14-17]. Results disclosed that the identified triazolyl-indole bearing sulfanyl moiety as lead molecules were efficiently impeding cell migration and cell proliferation, potentially by interfering with polymerase 1 (PARP-1) [15], or tyrosine kinases (EGFR, PI3, and Akt) enzymes activities [16,17]. In addition to this, the triazolyl-indole scaffold employed for fluorimetric DNA biosensor assay as a novel fluorophore for detection suppressor gene of the tumor disclosed in 2018 by the research group of Darestani-Farahani [18]. Many of other synthesized triazolyl-indole scaffolds were found to display strong antibacterial activities (S. aureus and

E. coli) [19], DPPH scavenger capacity [20], and as inhibitor for staphylococcal biofilms [21].

Further utilization for the triazolyl-indole scaffold has been reported as a fluorescent probe application for Al^{3+} ions [22], and in chemical organic processes, especially organometallic complexes as catalysts for Mizrachi–Heck, and Tsuji–Trost reaction catalysis [23]. In addition, 1,2,4-triazole moiety is a main building block in the skeletons of many approved drugs [24,25]. Leading examples are the well-known antimigraine agent (rizatriptan), antiviral agent (ribavirin), anxiolytic agent (alprazolam), antifungal agents (fluconazole, itraconazole, and terconazole) are the well-known of potent drugs incorporating a triazole motif. To design and construct, then characterization a new hybrid with chemical insight investigations is a highly challenge of research interest.

According to that finding and further proceeding in our research program [26,27] we have reported here the synthesis of two hits of the triazolyl-indole containing sulfanyl moiety. The structures of the two hits are assigned based on single crystal X-ray diffraction analysis along with ^{1}H and ^{13}C NMR spectral analysis. The molecular investigations were also included Hirshfeld surface analysis; NBO and DFT.

Experimental

General

"Melting points are uncorrected and measured using a melting-point apparatus (SMP10) in open capillaries. ^{1}H and ^{13}C NMR and 2D NMR spectra were recorded using a Brucker 300 MHz spectrometer in DMSO-d_6 using TMS as internal standard. Mass spectra were recorded on JMS-600H JEOL spectrometer. λ_{max} was measured using T90 + UV/VIS spectrometer".

Alkylation procedure for the synthesis of **2** and **3**

A mixture of 4-amino-5-(1*H*-indol-2-yl)-1,2,4-triazol-3(2*H*)-thione **1** (1.0 mmol) and Et_3N (1.2 mmol) in abs. EtOH was stirred for 1 h at rt. Subsequently, the appropriate halo-ester

(1.1 mmol) was added then the reaction mixture continued overnight under stirring, the excess ethanol was removed and cold water was added. The solid precipitate was collected and dried. Recrystallization of crudes from ethanol to afford the pure crystalline products suitable for x-ray diffraction analysis.

***tert*-Butyl 2-((4-amino-5-(1*H*-indol-2-yl)-4*H*-1,2,4-triazol-3-yl)thio)acetate 2**

Yield: 89%, m.p. 209 ^{o}C (decomp.); ^{1}H NMR (DMSO-d_6, 300 MHz) δ 1.40 (s, 9 H, $SCH_2COOC[CH_3]_3$), 3.99 (s, 2 H, SCH_2), 6.28 (s, 2 H, NH_2), 7.03 (dd, 1 H, $J_{4,5}$ 7.8, $J_{5,6}$ 7.1 Hz, H-5_{Indol}), 7.16 (dd, 1H, $J_{5,6}$ 7.1, $J_{6,7}$ 8.1 Hz, H-6_{Indol}), 7.28 (d, 1 H, J 1.2 Hz, H-3_{Indol}), 7.44 (d, 1 H, $J_{6,7}$ 8.1 Hz, H-7_{Indol}), 7.61 (d, 1 H, $J_{4,5}$ 7.8 Hz, H-4_{Indol}), 11.76 (br. s, 1H, NH_{Indol}); ^{1}C NMR (DMSO-d_6, 75 MHz) δ 27.61 ($3CH_3$), 34.11 (SCH_2), 81.42 ($C_{(CH3)3}$), 102.27 (C-3_{Indol}), 111.83 (C-7_{Indol}), 119.61 (C-5_{Indol}), 120.77 (C-4_{Indol}), 122.84 (C-6_{Indol}), 123.86 (C-2_{Indol}), 127.58 (C-$3a_{Indol}$), 136.49 (C-$7a_{Indol}$), 149.34 (C-$5_{ind\text{-}Triazol}$), 152.65 (C-$3_{Triazol}$-s), 167.51 (C=O); HRMS (EI) calcd for $C_{16}H_{19}N_5SO_2$ (M^+): 345.1259. Found: 345.1252.

Ethyl 2-((4-amino-5-(1*H*-indol-2-yl)-4*H*-1,2,4-triazol-3-yl)thio)acetate 3

Yield: 77 %, m.p. 210-211 ^{o}C; ^{1}H NMR (DMSO-d_6, 300 MHz) δ 1.20 (t, 3 H, J 7.1 Hz, $SCH_2COOCH_2CH_3$), 4.10-4.14 (m, 4 H, $SCH_2COOCH_2CH_3$), 6.29 (s, 2 H, NH_2), 7.03 (dd, 1 H, $J_{4,5}$ 7.9, $J_{5,6}$ 7.2 Hz, H-5_{Indol}), 7.16 (dd, 1H, $J_{5,6}$ 7.2, $J_{6,7}$ 8.1 Hz, H-6_{Indol}), 7.27 (d, 1 H, J 1.2 Hz, H-3_{Indol}), 7.45 (d, 1 H, $J_{6,7}$ 8.1 Hz, H-7_{Indol}), 7.61 (d, 1H, $J_{4,5}$ 7.9 Hz, H-4_{Indol}), 11.73 (br. s, 1H, NH_{Indol}); ^{13}C NMR (DMSO-d_6, 75 MHz) δ 13.97 ($SCH_2COOCH_2CH_3$), 33.05 ($SCH_2COOCH_2CH_3$), 61.16 ($SCH_2COOCH_2CH_3$), 102.30 (C-3_{Indol}), 111.82 (C-7_{Indol}), 119.60 (C-5_{Indol}), 120.73 (C-4_{Indol}), 122.83 (C-6_{Indol}), 123.79 (C-2_{Indol}), 127.55 (C-$3a_{Indol}$), 136.47 (C-$7a_{Indol}$), 149.38 (C-$5_{ind\text{-}Triazol}$), 152.63 (C-$3_{Triazol}$-s), 168.47 (C=O); HRMS (EI) calcd for $C_{14}H_{15}N_5SO_2$ (M^+): 317.0943. Found: 317.0946.

X-Ray structural determinations

The crystals of **2** and **3** were immersed in cryo-oil, mounted in a loop, and measured at a temperature of 120 K. The X-ray diffraction data were collected on a Rigaku Oxford Diffraction Supernova diffractometer using Mo Kα (**2**) or Cu Kα (**3**) radiation. The *CrysAlisPro* [28] software package was used for cell refinements and data reductions. An analytical (**2**) or multi-scan (**3**) absorption correction (*CrysAlisPro* [28]) was applied to all data. The structures were solved by intrinsic phasing method using the *SHELXT* [29] software. Structural refinements were carried out using *SHELXL* [29] software with *SHELXLE* [30] graphical user interface. The unit cell of **3** contains two independent molecules. The ester tail of one of the molecules was disordered over two sites with

occupancy ratio of 0.52/0.48. Due to the disorder a series of geometric and displacement constraints and restraints were applied to the disordered atoms. The NH and NH_2 hydrogen atoms were located from the difference Fourier map and refined isotropically. Other hydrogen atoms were positioned geometrically and constrained to ride on their parent atoms with C-H = 0.95-0.99 Å and U_{iso} = 1.2-1.5 U_{eq} (parent atom). The crystallographic details are summarized in Table **1**.

Hirshfeld surface analysis

The topology analyses were performed using Crystal Explorer 17.5 program [31].

Computational methods

"The B3LYP/6-31G(d,p) method were employed using Gaussian 09 software package for all DFT calculations [32]. The resulting optimized structures showed no imaginary frequencies. NBO 3.1 program as implemented in the Gaussian 09W package used for natural population analysis [33]. The self consistent reaction filed (SCRF) method [34, 35] was used to model the solvent (DMSO) effects when calculated the optimized geometries in solution. Then the NMR chemical shifts for the protons and carbons were computed using GIAO method in the same solvent (DMSO) [36]. Similarly, the structure was optimized in solution of compound using ethanol as solvent then the optimized molecular structure was used to calculate the electronic spectra using the time-dependant density functional theory (TD-DFT)."

Results and discussion

Coupling of 4-amino-5-(1*H*-indol-2-yl)-1,2,4-triazol-3(2*H*)-thione **1** with *tert*-butyl bromoacetate and ethyl chloroacetate was done in the presence of Et_3N as a proton scavenger in ethanol as a solvent and stirring overnight (Scheme 1). The products were purified by recrystallization and the alkylation direction and selectivity were assigned using NMR.

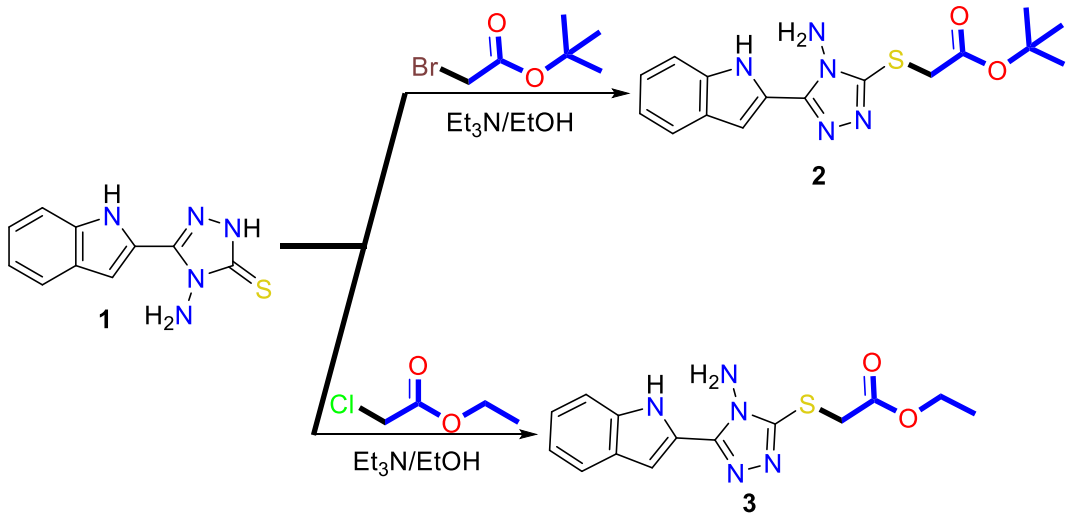

Scheme 1. Synthesis of the alkyl sulfanyl-5-(1*H*-indol-2-yl)-1,2,4-triazole derivatives **2** and **3**

Structural Characterization

The ^{1}H NMR spectra of the alkylated products **2** and **3** showed the indole ring protons around δ 7.03, 7.16, 7.28, 7.44 and 7.61 ppm. The amino group protons (NH_2) were found at δ 6.28 ppm which the indole NH proton was detected at δ 11.76 ppm. The ^{13}C NMR spectra displayed the aromatic CH carbons at δ 102.27, 111.83, 119.61, 120.77 and 122.84 ppm. The aromatic quaternary carbons were found at δ 123.86, 127.58, 136.49, 149.34 and 152.65 ppm. Compounds **2** and **3** showed a characteristic signals showing the difference in the alkylating part: the target compound **2** revealed the *tert*-butyloxy protons ($OC(CH_3)_3$) at δ 1.40 ppm and the methylene CH_2 protons at 3.99 ppm. The *tert*-butyloxy carbon signals were detected at δ 27.61, and 81.42 ppm. The methylene protons (CH_2) were found at δ 34.11 ppm. The carbonyl carbon (C=O) was appeared at δ 167.51 ppm. The hit compound **3** revealed that the methyl protons at δ 1.20 ppm whereas, the methylene protons SCH_2 and OCH_2 were detected between δ 4.10-4.14 ppm. The ethoxy group carbons were found at δ 13.97, and 61.16 ppm. The remaining methylene carbon appeared at δ 33.05 ppm while the carbonyl carbon was detected at 168.47 ppm. The methylene carbon signals that found at δ 34.11 ppm in **2** and δ 33.05 ppm in **3** is strong evidence that the alkylations were done on sulfur not nitrogen.

^{1}H-^{1}H Correlation Spectroscopy (COSY) helped in confirmation the position of the indole ring adjacent protons that displayed $^{3}J_{H,H}$ coupling correlations between the protons at δ 7.61 and 7.03 ppm, the later also correlated with the proton at δ 7.16 ppm this proton also coupled with the proton at δ 7.44 ppm. The 2D HMQC NMR was used to detect the correlation and position of each CH, CH_2 and CH_3 (Figure 1).

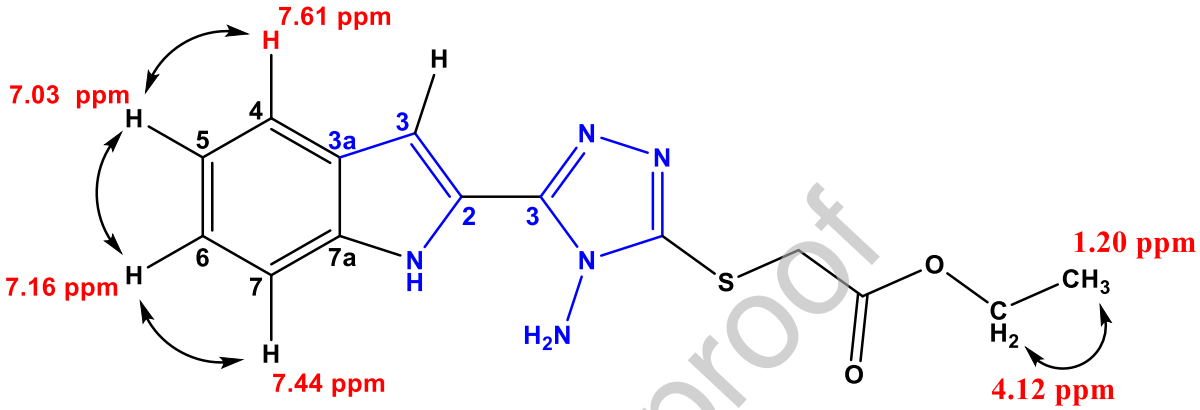

Figure. 1 2D COSY Schematic representation of **3**

X-Ray structure descriptions

The crystal data and processing parameters for **2** and **3** are given in **Table 1**. Both compounds are crystallized in the triclinic crystal system and the primitive P $\bar{1}$ space group with two and four molecules per unit cell for **2** and **3**, respectively. In case of **2**, there is one molecule per asymmetric unit while in **3** there are two molecules per asymmetric unit. Full geometric parameters such as bond distance, angles and torsion angles are given in **Tables S1-S5** (Supplementary data).

Table 1. Crystal Data.

	2	**3**
empirical formula	$C_{16}H_{19}N_5O_2S$	$C_{14}H_{15}N_5O_2S$
fw	345.42	317.37
temp (K)	120(2)	120(2)
λ(Å)	1.54184	0.71073
cryst syst	Triclinic	Triclinic
space group	P $\bar{1}$	P $\bar{1}$
a (Å)	5.43580(10)	5.9924(2)
b (Å)	10.4214(3)	8.7769(3)
c (Å)	14.8371(3)	29.2084(11)
α (deg)	83.652(2)	83.015(3)

β (deg)	82.777(2)	85.989(3)
γ (deg)	81.663(2)	72.681(3)
V (Å^3)	821.36(3)	1454.75(9)
Z	2	4
ρ_{calc} (Mg/m^3)	1.397	1.449
μ(Mo Kα) (mm^{-1})	1.922	0.238
No. reflns.	18594	10357
Unique reflns.	3440	6407
GOOF (F^2)	1.066	1.045
R_{int}	0.0344	0.0353
R_1[a] ($I \geq 2\sigma$)	0.0319	0.0526
wR_2[b] ($I \geq 2\sigma$)	0.0871	0.1159
CCDC	2012727	2012728

[a] $R_1 = \Sigma||F_o| - |F_c||/\Sigma|F_o|$. [b] $wR_2 = [\Sigma[w(F_o^2 - F_c^2)^2]/ \Sigma[w(F_o^2)^2]]^{1/2}$.

The X-ray structure of **3** with thermal ellipsoids drawn at 50% probability level is shown in **Fig. 2 (upper part)**. The molecule comprised two planar aromatic π-systems; the indole and triazole moieties connected by C8-C9 bond. The mean plane passing through the indole moiety make an angle of about 7º with the triazole ring mean plane indicating the presence of some twist for the two ring systems from one another (**Fig. 2, lower part**).

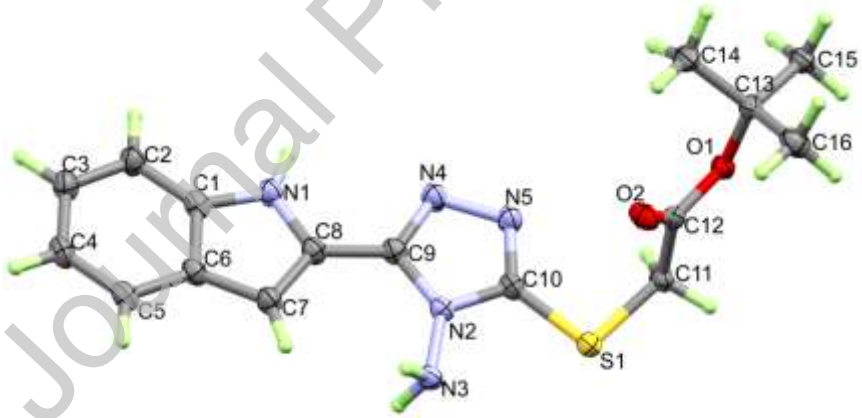

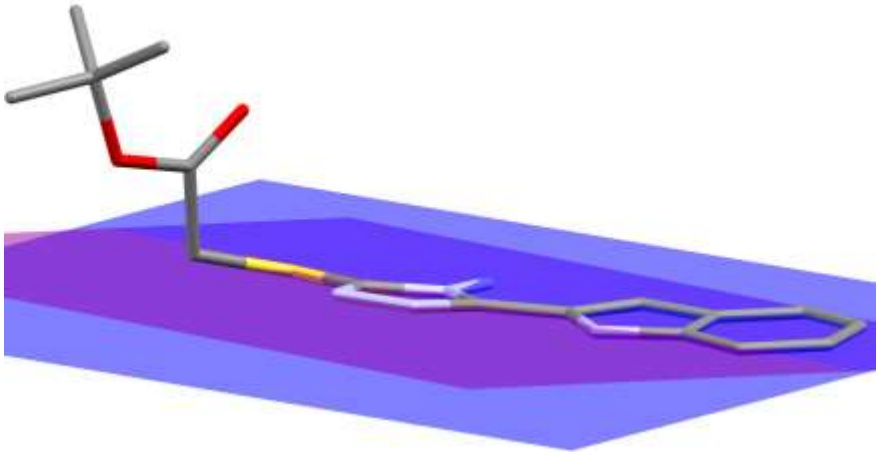

Fig. 2 X-ray structure (upper) and the mean plane of the indole (blue) and triazole (magenta) moieties showing the twist among them (lower) in **3**.

The molecules of **2** are packed in the three dimensions *via* the hydrogen bonding interactions shown in **Fig. 3** and listed in **Table 2**. The molecules are packed *via* N-H...S, N-H...O and N-H...N hydrogen bonds as well as some weak C-H...O and C-H...N interactions. Interestingly, the second proton (H3B) of the NH_2 group is not participating in any significant hydrogen bonding interactions but included in some N-H...π interactions with the C5 and C6 atoms from the indole moiety with C...H contact distances of 2.757(2) and 2.548(2) Å, respectively.

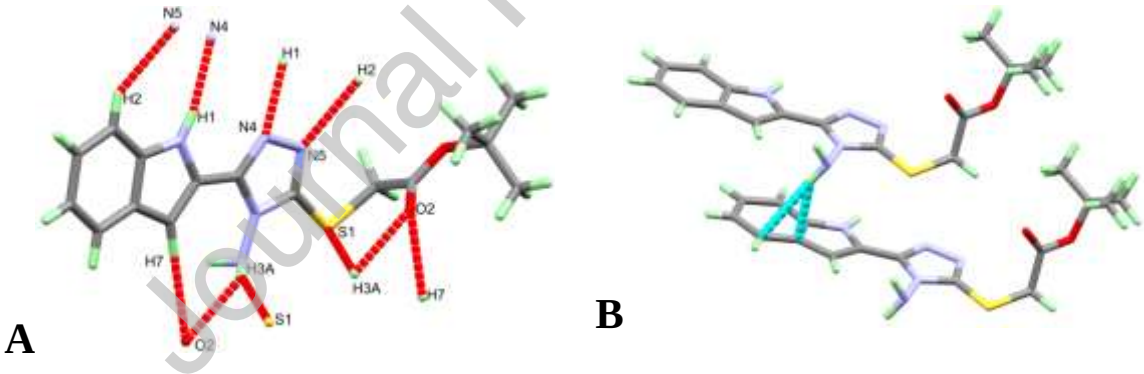

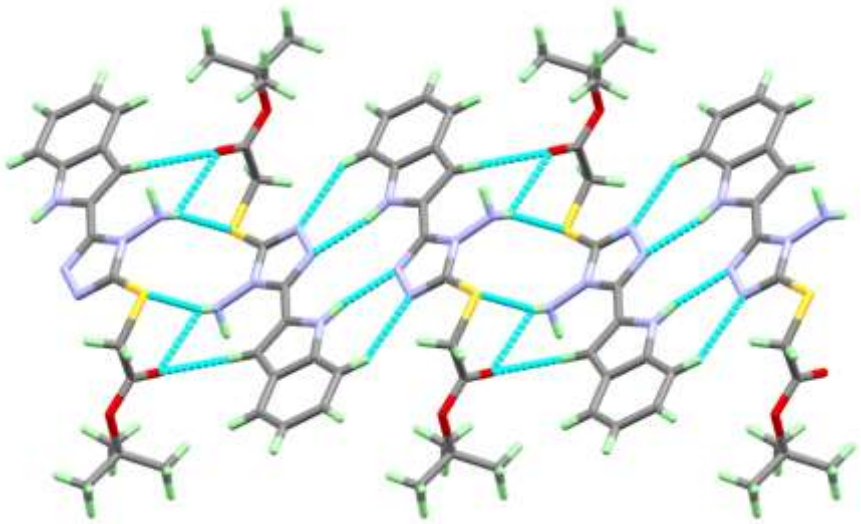

C

Fig. 3 Hydrogen bond contacts (**A**), N-H...π interactions (**B**) and hydrogen bonding polymer (**C**) in **2**.

Table 2 Hydrogen bonds for **2** [Å and °].

D-H...A	d(D-H)	d(H...A)	d(D...A)	<(DHA)
C7-H7...O2$^{\#1}$	0.95	2.51	3.4585(16)	174.7
C2-H2...N5$^{\#2}$	0.95	2.48	3.2805(17)	142.4
N3-H3A...S1$^{\#1}$	0.908(19)	2.670(19)	3.5531(12)	164.4(15)
N3-H3A...O2$^{\#1}$	0.908(19)	2.369(17)	2.9172(14)	118.8(13)
N1-H1...N4$^{\#2}$	0.85(2)	2.14(2)	2.9616(16)	163.4(17)

#1 -x,-y+1,-z+1 #2 -x+1,-y,-z+1

The X-ray structure of **3** is given in **Fig. 4**. Similar to **2**, the two planar indole and triazole moieties are not perfectly coplanar with each other in both asymmetric formulas. The degree of the twist between the two rings is higher (9.24º) in case of molecule **B** but lower in molecule **A** (3.05 º) than that in **2.**

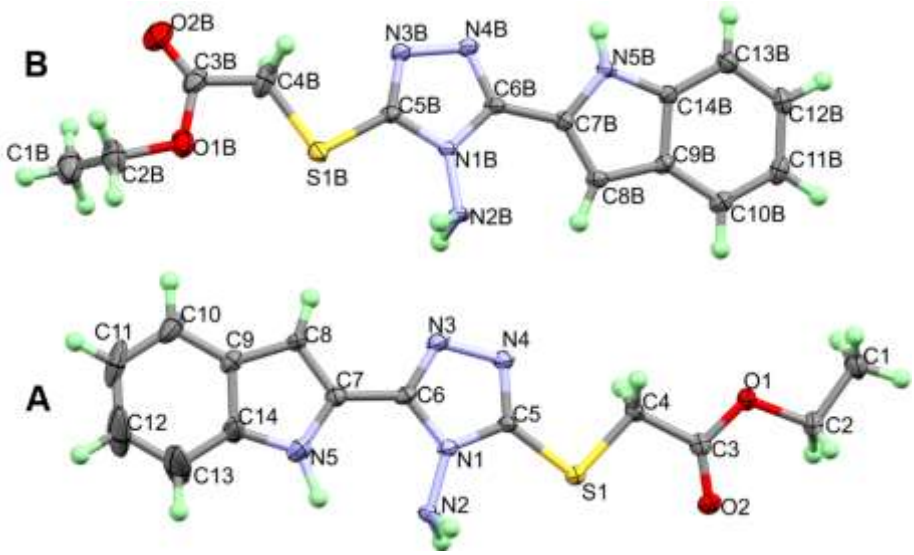

Fig. 4 X-ray structure at 50% probability level of **3**.

The molecules of **3** are also packed in the crystal structure *via* the strong N-H...N, N-H...S, N-H...O hydrogen bonds and weak C-H...O interactions shown in the upper part of **Fig. 5**. Summary of these contacts along with the hydrogen bond parameters are listed in **Table 3**, while the hydrogen bond network is shown in the lower part of **Fig. 5**.

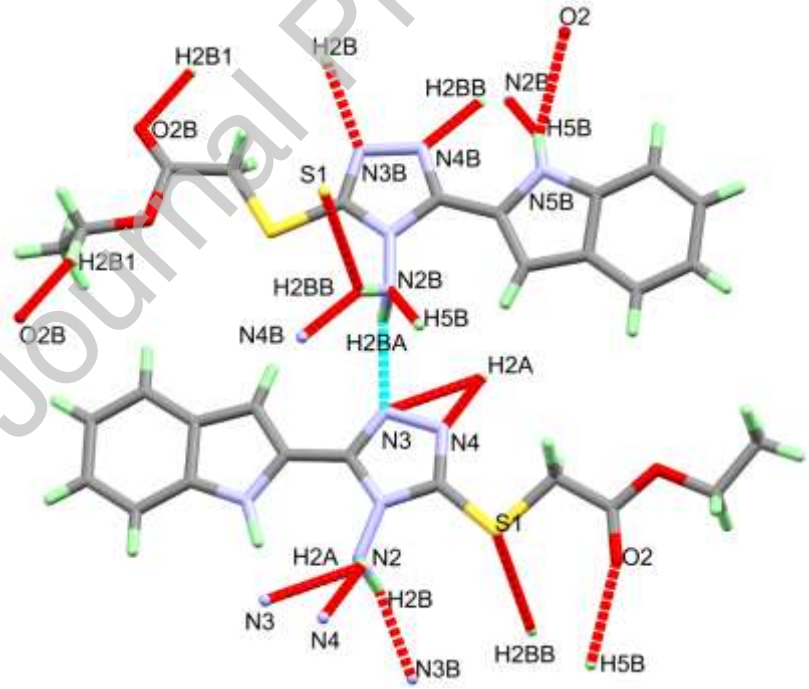

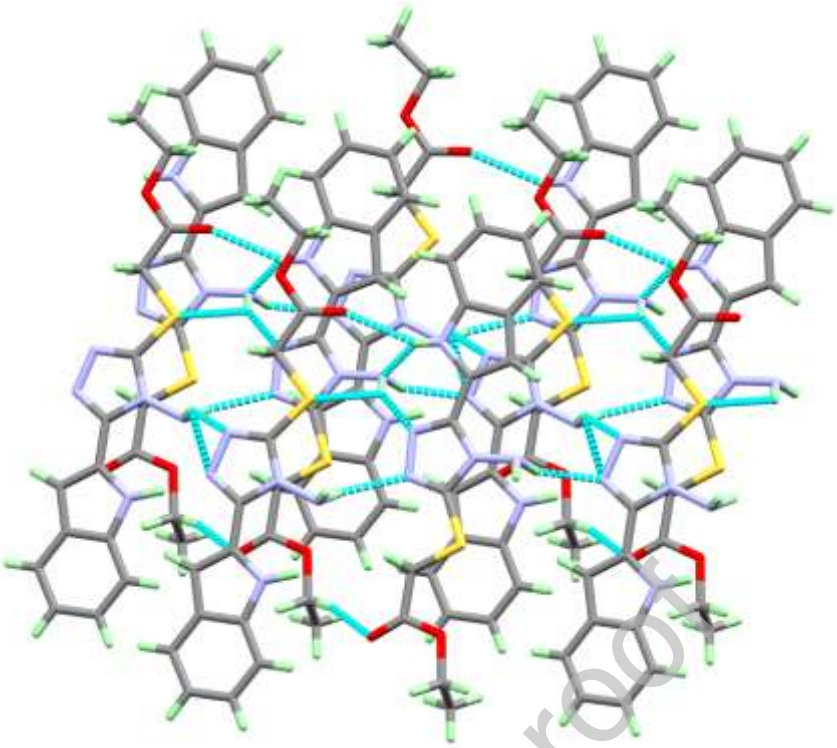

Fig. 5 Hydrogen bond contacts (upper) and hydrogen bonding polymer (lower) in **3**.

Table 3: Hydrogen bonds for **3** [Å and °].

D-H...A	d(D-H)	d(H...A)	d(D...A)	<(DHA)
N2-H2A...N3$^{\#1}$	0.95(3)	2.65(3)	3.189(3)	117(2)
N2-H2A...N4$^{\#1}$	0.95(3)	2.18(3)	2.985(3)	142(2)
N2-H2B...N3B$^{\#2}$	0.92(3)	2.16(3)	2.965(3)	145(2)
N2B-H2BA...N3	0.96(3)	2.10(3)	2.886(3)	138(2)
N2B-H2BB...S1$^{\#3}$	0.91(3)	2.95(3)	3.560(3)	125(3)
N2B-H2BB...N4B$^{\#1}$	0.91(3)	2.10(3)	2.940(3)	152(3)
N5B-H5B...O2$^{\#4}$	0.80(4)	2.44(4)	3.142(3)	147(3)
N5B-H5B...N2B$^{\#5}$	0.80(4)	2.70(3)	3.219(3)	124(3)
C2B-H2B1...O2B$^{\#1}$	0.99	2.45	3.413(10)	163.6
#1 x+1,y,z #2 x+1,y+1,z	#3 x,y-1,z	#4 x-1,y-1,z , #5 x-1,y,z		

Analysis of molecular packing

The different contacts observed in the crystal structure of **2** are shown in **Fig. 6** while list of the interaction distances is given in **Table 4**. The molecules are mainly packed by many strong interactions such as O...H (9.3%), N...H (12.4%) and S...H (3.1%) as well as relatively weak C...H (14.1%), S...C (2.1%), H...H (50.5%) and S...S (0.9%) contacts. The decomposed d_{norm} maps and fingerprint plots are shown in **Fig. 7**. These contacts have less interaction

distances than vdW radii sum of the interacting atoms. Also, all appeared as red spots in the d_{norm} map.

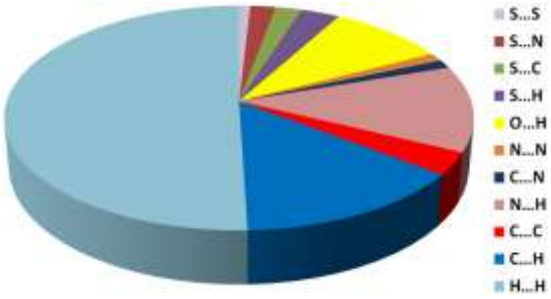

Fig. 6 The percentages of all contacts in **2**.

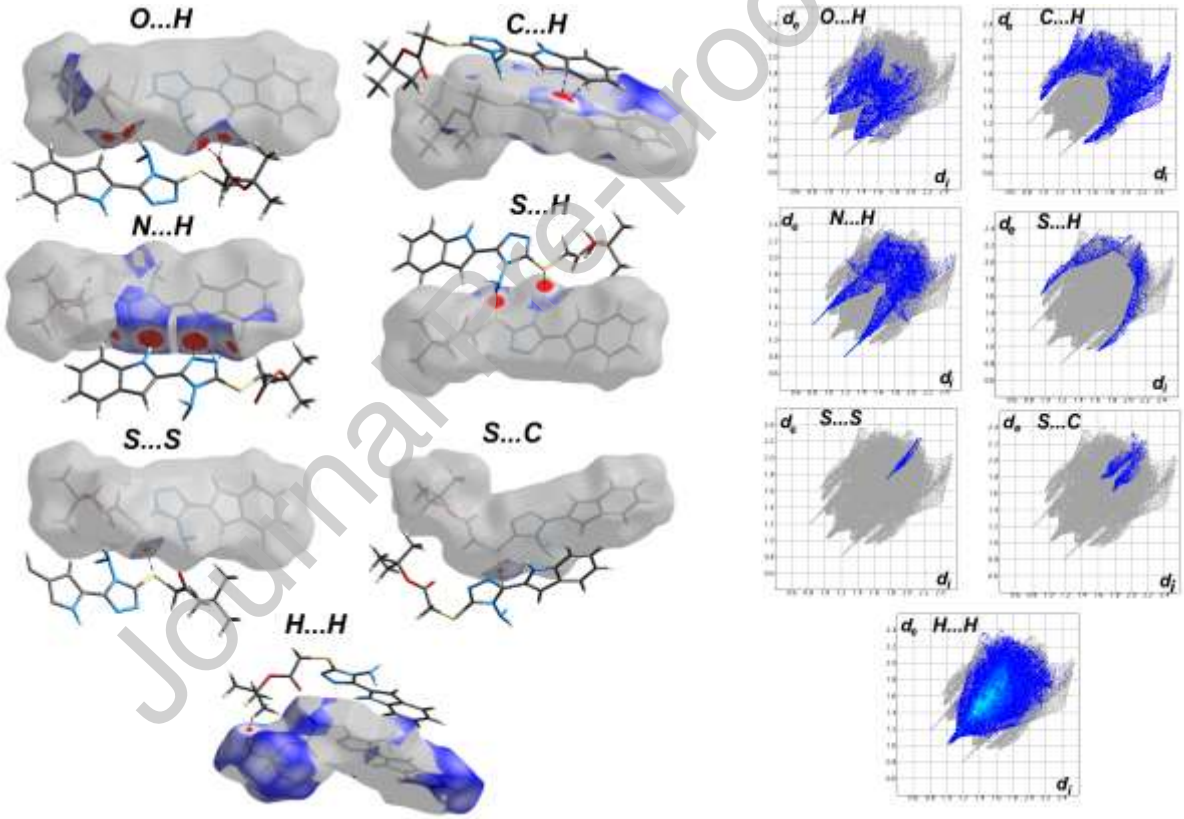

Fig. 7 Hirshfeld surfaces of all important contacts in **2**.

Table 4 The short intermolecular contacts in **2**.

Contact	Distance	Contact	Distance
N4…H1	1.985	C9…S1	3.407
N5…H1	2.62	S1…S1	3.488
N5…H2	2.373	C6…H3B	2.453

O2...H3A	2.322	C5…H3B	2.64
O2…H7	2.379	H15A…H14B	2.051
S1...H3A	2.573		

For **3**, the asymmetric unit comprised two molecules of this compound. For simplicity, we labelled the two molecular units as molecules A and B as shown in **Fig. 4**. As a result, there are two results for the Hirshfeld quantitative analysis as shown in **Fig. 8**. In this case, the molecules are packed by strong O...H (11.0-12.3%) and N...H (13.1-13.6%) hydrogen bonds as well as weak C...H (15.3-16.4%), S...N (0.8-1.7%) and H...H (43.6-43.9%) interactions. Those having short interaction distances are presented in **Fig. 9**. List of the interaction distances is given in **Table 5**. The strongest contacts appeared as red spots which corresponding to O…H and N…H hydrogen bonds.

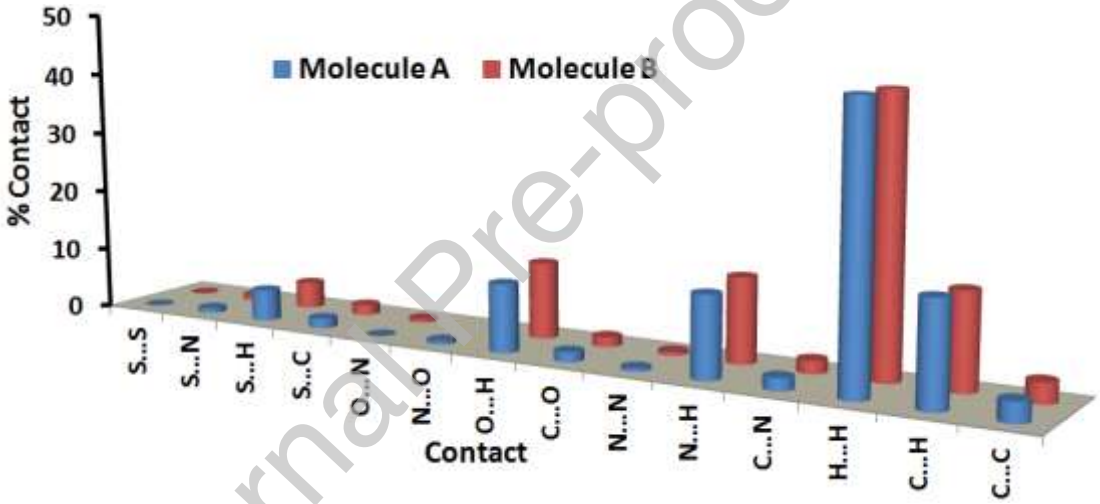

Fig. 8 Summary of the intermolecular interactions and their percentages in the crystal structure of **3.**

Table 5 The short intermolecular contacts in **3**.

Contact	Distance	Contact	Distance
N4B…H2BB	2.020	S1…N4B	3.337
N3…H2BA	2.064	O2…H5B	2.269
N2B…H5B	2.586	O2B…H2B1	2.363
N3…H2A	2.618	H10…H1B3	2.131
N4…H2A	2.135	C9B…H2C	2.789
N3B…H2B	2.088	C14B…H2C	2.708
N3…H2A	2.818	C14…H2B2	2.601
N4…H2A	2.135		

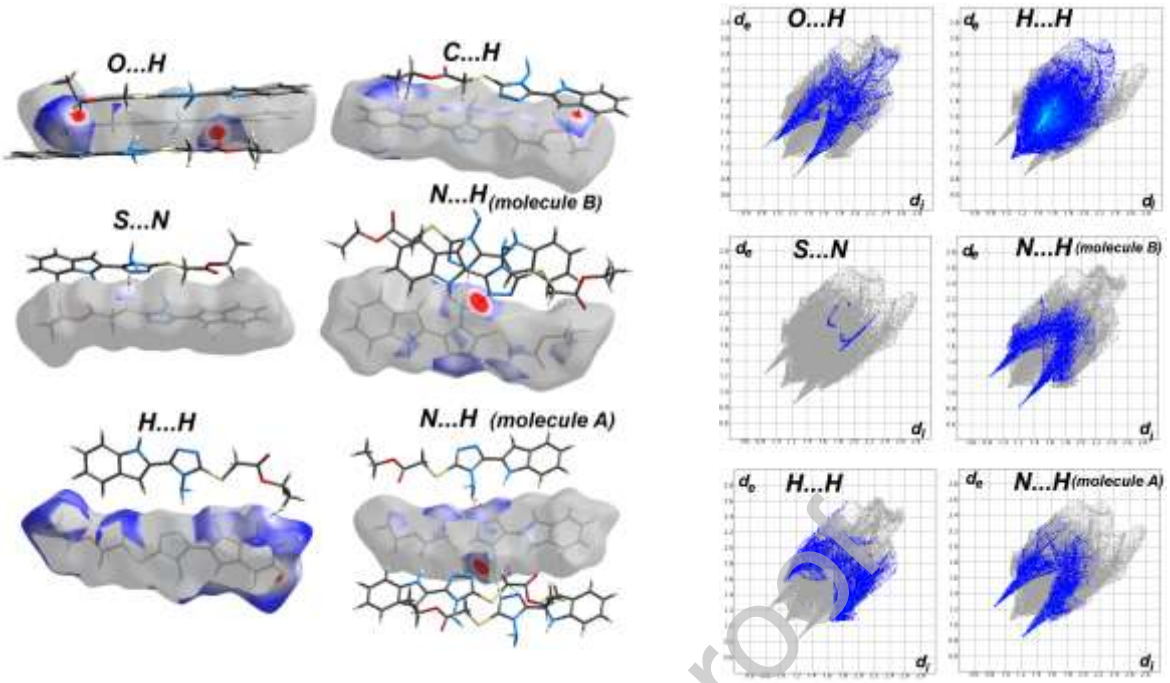

Fig. 9 The decomposed d_{norm} maps (left) and fingerprint plots (right) of all contacts with shorter distance than the vdW radii sum of the interacting atoms for **3**. The N...H contacts repeated twice because the N...H interactions in both molecules in the asymmetric unit are not the same while the rest of contacts are common in both molecules.

DFT Studies

Geometric parameters

The optimized molecular geometries of **2** and **3** compounds compared with the X-ray structure model are given in **Fig. 10**. There are good correlations between the optimized and X-ray structure bond distances for both compounds (**Fig. 11**) which indicate the good agreement between the optimized and calculated bond distances **(Table S6, Supplementary data)**. The correlation coefficients are 0.9967 and 0.9791, respectively. Both compounds are polar where the calculated dipole moment values are 0.980 and 5.029 Debye for **2** and **3**, respectively indicating the higher polarity for the ethyl ester (**3**) than the *t*-butyl ester (**2**).

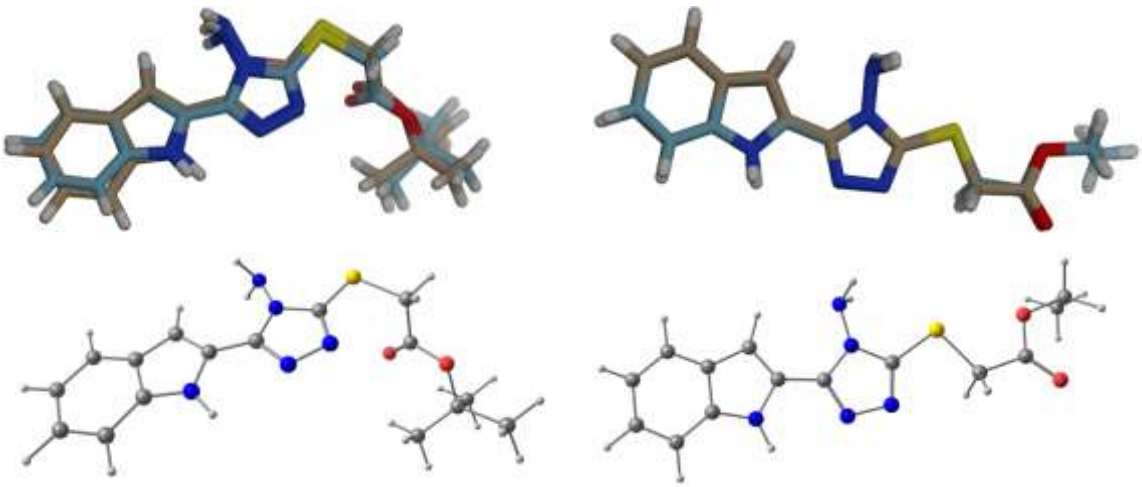

2 **3**

Fig. 10 Optimized structures (lower) and structure matching (upper) between the calculated and experimental structures of **2** and **3**.

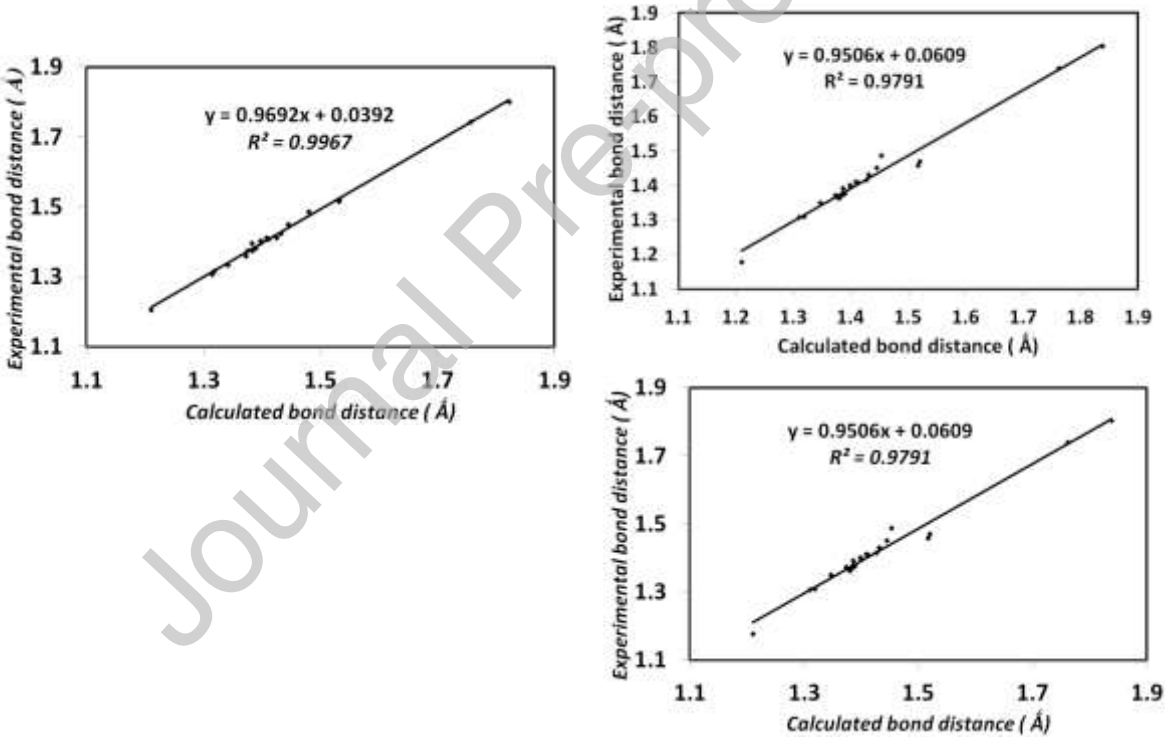

2 **3**

Fig. 11 Correlation between the calculated and experimental bond distances of **2** and **3**

The natural charges at the different atomic sites are listed in **Table S7 (Supplementary data)**. The most negative atomic sites are the oxygen and nitrogen atoms in both compounds. On other hand, the most positive sites are the NH and NH_2 protons. Molecular electrostatic potential (MEP) map is a colored presentation that indicates the different charged regions in

molecular systems. Red colored regions are the most negative while the most positive regions have blue color (**Fig. 12**). These regions represent the most proper regions for hydrogen bonding interactions as hydrogen bond acceptor and hydrogen bond donor, respectively. The red regions are related to the carbonyl oxygen and the two sp^2 hybridized nitrogen atoms in the triazole moiety. Those represent the most suitable regions for hydrogen bonding interactions as hydrogen bond acceptor sites. In contrast, the blue regions are related to the protons of the amino groups (NH_2 and NH) which act as hydrogen bond donor. These results are in good agreement with the X-ray structure of the studied compounds.

2 **3**

Fig. 12 The MEP maps of **2** and **3**.

Reactivity studies

The reactivity indices of the studied compounds such as ionization potential (I), electron affinity (A), chemical potential (μ), hardness (η) as well as electrophilicity index (ω) were calculated [37-44] and the results are listed in **Table 6**.

Table 6 The calculated reactivity indices of the studied compounds.

Parameter	2	3
HOMO	-5.4872	-5.3471
LUMO	-1.0901	-0.9206
I	5.4872	5.3471
A	1.0901	0.9206
η	4.3971	4.4265
μ	-3.2887	-3.1338
ω	1.2298	1.1093

It is clear that the reactivity descriptors for both compounds are almost identical. Also, the reactivity descriptors are not affected by the type of alkyl moiety attached to the carboxylate group. For example, the ionization potential (5.4872 eV) and electron affinity (1.0901 eV) are

slightly higher for **2** than those for **3** (5.3471 and 0.9206 eV, respectively). Similarly, the electrophilicity is higher (1.2298 eV) for the former than the latter (1.1093 eV).

The HOMO and LUMO levels are shown in **Fig. 13**. In both cases, the HOMO is mainly localized over the triazole moiety and sulphur atom while the LUMO is localized over the whole heterocyclic π-system. Since, the pattern of the HOMO and LUMO indicate the regions responsible for the intramolecular charge transfer transitions, hence the HOMO→LUMO intramolecular charge transfer could be described as mixed π-π* and n-π* transitions with transition energies of 4.397 and 4.427 eV for **2** and **3**, respectively.

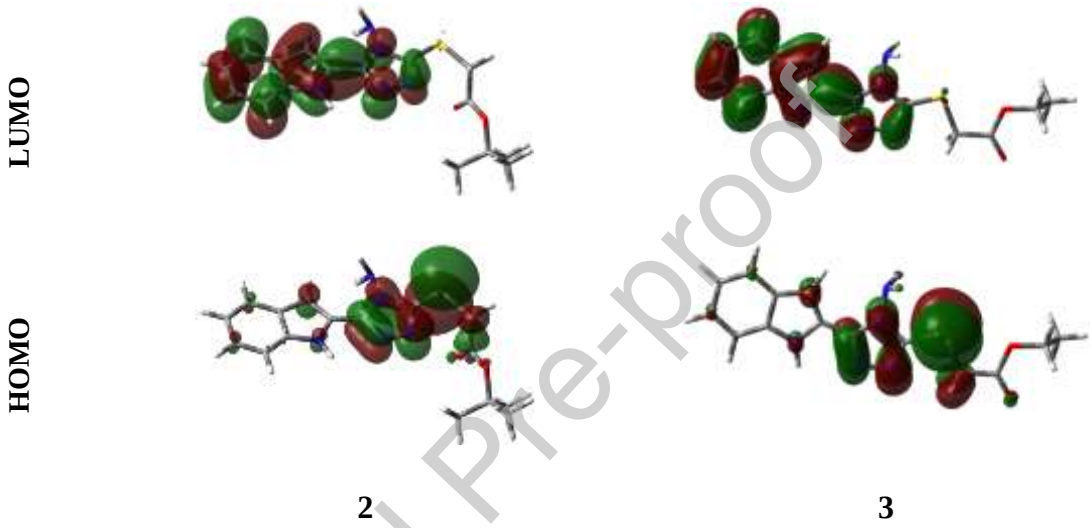

Fig. 13 HOMO and LUMO presentation of **2** and **3**.

NBO analysis

The strength of electron delocalization processes in the studied molecules is analyzed using second order perturbation theory [45, 46]. It sheds the light on the different electron delocalization processes which stabilize the molecular system. The stabilization energy ($E^{(2)}$) listed in **Table 7** indicate the extent of electron delocalization processes [45]. The system is stabilized by different types of intramolecular charge transfer interactions such as σ→σ*, π→π*, n→σ* and n→π* electron delocalization processes. The energies of these charge transfer interactions stabilized the studied molecules up to 6.96, 19.55, 32.44 and 52.73 kcal/mol respectively for **3**. On other hand, the corresponding values for **4** are 7.47, 19.89, 33.31 and 48.42 kcal/mol, respectively.

Table 7 The stabilization $E^{(2)}$ (kcal/mol) for the electron delocalization processes in the studied compounds [a].

Donor NBO	Acceptor NBO 2	$E^{(2)}$	Donor NBO	Acceptor NBO 3	$E^{(2)}$
σ→σ*					
BD(1)N6-N8	BD*(1)S1-C11	6.96	BD(1)N6-N7	BD*(1)S1-C10	7.47
BD(1)N6-N8	BD*(1)C9-C16	5.86	BD(1)N6-N7	BD*(1)C11-C12	5.61
BD(1)C9-C12	BD*(1)C10-C25	5.10	BD(1)C12-C13	BD*(1)C15-C16	5.23
BD(1)C10-C12	BD*(1)C9-C16	6.80	BD(1)C20-C22	BD*(1)N8-C24	6.15
π→π*					
BD(2)N6-C11	BD*(2)N8-C16	13.02	BD(2)N6-C10	BD*(2)N7-C11	11.77
BD(2)N8-C16	BD*(2)N6-C11	12.86	BD(2)N7-C11	BD*(2)N6-C10	13.71
BD(2)N8-C16	BD*(2)C9-C12	11.46	BD(2)N7-C11	BD*(2)C12-C13	10.51
BD(2)C9-C12	BD*(2)N8-C16	18.10	BD(2)C12-C13	BD*(2)N7-C11	19.89
BD(2)C9-C12	BD*(2)C10-C15	15.83	BD(2)C12-C13	BD*(2)C15-C24	15.93
BD(2)C10-C15	BD*(2)C9-C12	18.90	BD(2)C15-C24	BD*(2)C12-C13	18.93
BD(2)C10-C15	BD*(2)C17-C27	17.84	BD(2)C15-C24	BD*(2)C16-C18	19.24
BD(2)C10-C15	BD*(2)C20-C25	19.02	BD(2)C15-C24	BD*(2)C20-C22	17.91
BD(2)C17-C27	BD*(2)C10-C15	19.55	BD(2)C16-C18	BD*(2)C15-C24	16.34
BD(2)C17-C27	BD*(2)C20-C25	17.06	BD(2)C16-C18	BD*(2)C20-C22	19.42
BD(2)C20-C25	BD*(2)C10-C15	16.69	BD(2)C20-C22	BD*(2)C15-C24	19.34
BD(2)C20-C25	BD*(2)C17-C27	19.35	BD(2)C20-C22	BD*(2)C16-C18	16.84
n→σ*					
LP(1)S1	BD*(1)N6-C11	5.11	LP(1)S1	BD*(1)N6-C10	5.36
LP(2)S1	BD*(1)C14-C22	5.49	LP(1)O29	BD*(1)C28-O30	8.42
LP(1)O2	BD*(1)O3-C14	9.31	LP(2)O30	BD*(1)C28-O29	33.31
LP(2)O3	BD*(1)O2-C14	32.44	LP(2)O30	BD*(1)C25-C28	20.09
LP(2)O3	BD*(1)C14-C22	22.34	LP(1)N6	BD*(1)N2-C10	8.33
LP(1)N6	BD*(1)N5-C11	7.87	LP(1)N6	BD*(1)N7-C11	5.23
LP(1)N6	BD*(1)N8-C16	5.31	LP(1)N7	BD*(1)N6-C10	5.35
LP(1)N7	BD*(1)N5-C16	9.98	LP(1)N3	BD*(1)N2-C10	9.54
LP(1)N8	BD*(1)N5-C16	8.53			
LP(1)N8	BD*(1)N6-C11	5.38			
n→π*					
LP(2)S1	BD*(2)N6-C11	27.08	LP(2)S1	BD*(2)N6-C10	24.81
LP(2)O2	BD*(2)O3-C14	52.73	LP(2)O29	BD*(2)C28-O30	48.42
LP(1)N4	BD*(2)C9-C12	40.65	LP(1)N8	BD*(2)C12-C13	37.93
LP(1)N4	BD*(2)C10-C15	37.50	LP(1)N8	BD*(2)C15-C24	37.78
LP(1)N5	BD*(2)N6-C11	46.33	LP(1)N2	BD*(2)N6-C10	46.10
LP(1)N5	BD*(2)N8-C16	44.56	LP(1)N2	BD*(2)N7-C11	44.06

Uv-Vis and NMR spectra

The experimental UV-Vis electronic spectra of **2** and **3** in ethanol are shown in **Fig. 14**. It is clear that both compounds showed very similar electronic spectra. There are two bands observed at 242 and 307 nm, and two shoulders at 298 and 319 nm for both compounds. Theoretically, two well separated bands were observed. Their assignments compared with the experimental data are given in **Table 8**. The longest wavelength band was calculated at 303.7 nm (f=0.920) and 303.1 nm (f=0.885) for **2** and **3**, respectively. This band is assigned to HOMO→LUMO excitation with 97% contribution in both compounds. The shortest wavelength band observed at 242 nm was calculated at 232.0 (f=0.191) and 233.1 (f=0.187) for **2** and **3**, respectively. In the former, it is assigned to HOMO→LUMO+2 excitation with 80% contribution, while in the latter it is assigned to HOMO→LUMO+3 excitation (83%). The molecular orbitals included in these transitions are presented in **Fig. 15**.

Table 8 Assignment of the electronic spectra of the studied compounds.

$(\lambda_{max})_{calc.}$	f_{osc} [a]	Assignment	$(\lambda_{max})_{obs.}$
		2	
303.7	0.920	HOMO→LUMO (97%)	307
232.0	0.191	HOMO→L+2 (80%)	242
		3	
303.1	0.885	HOMO→LUMO (97%)	307
233.1	0.187	HOMO→L+3 (83%)	242

[a] oscillator strength

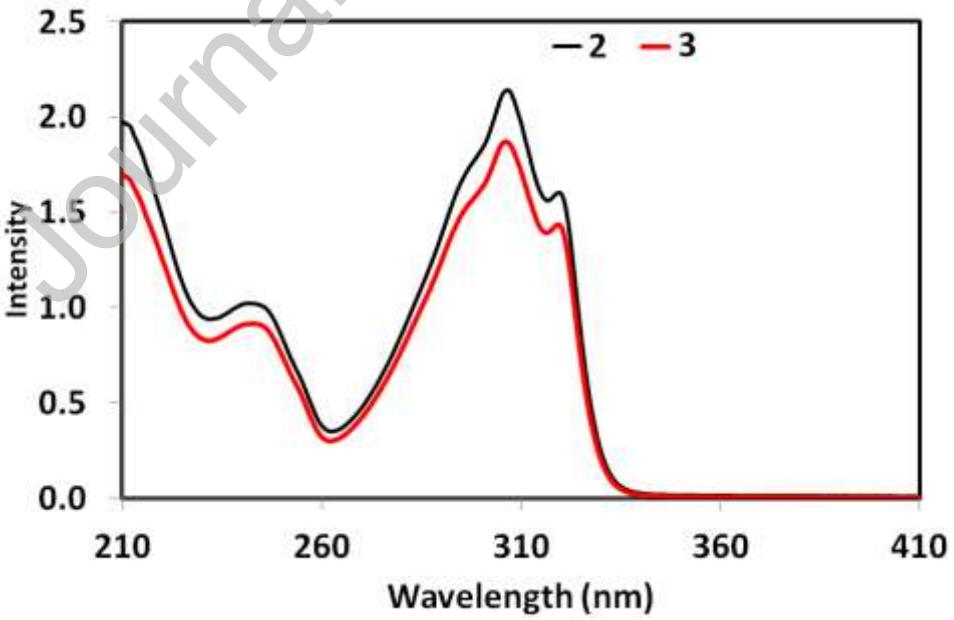

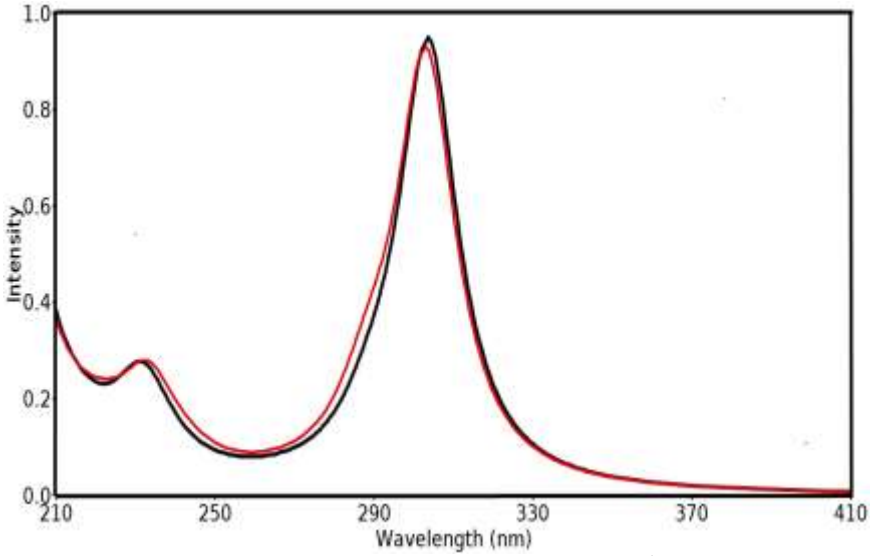

Fig. 14 The experimental (upper) and calculated (lower) UV-Vis electronic spectra of **2** and **3.**

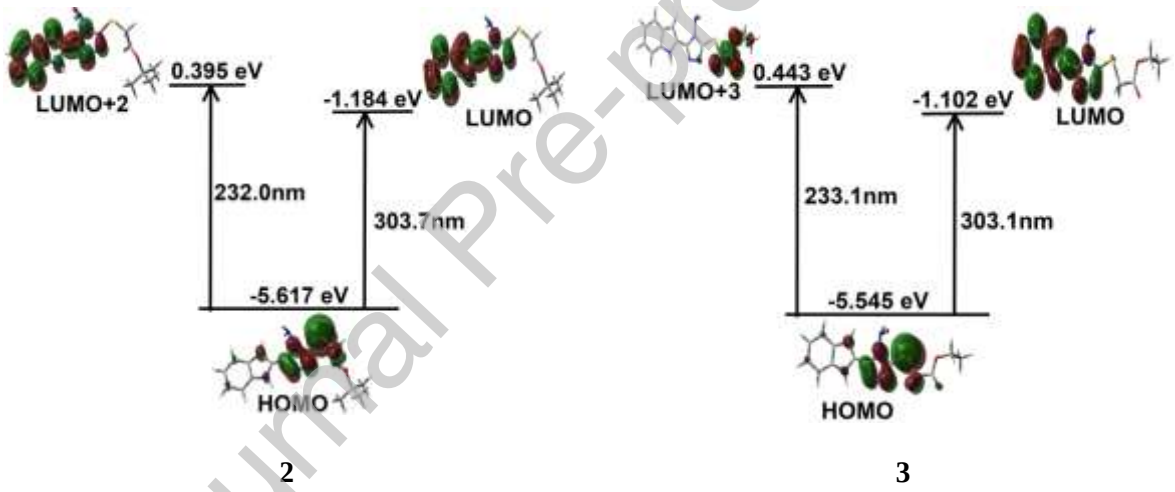

2 **3**

Fig. 15 Molecular orbitals incorporated in the electronic transitions of **2** and **3.**

The chemical shifts (C.S) of ^{1}H and ^{13}C were computed and the results are listed in **Table S7 (Supplementary data)** in comparison with the experimentally data. It is clear from **Fig. 16** that there is good relation between the experimental and calculated C.S values. For **2**, The correlation coefficients are 0.9771 for ^{1}H-NMR and 0.9955 for ^{13}C-NMR while the corresponding values for **3** are 0.9876 and 0.9958, respectively.

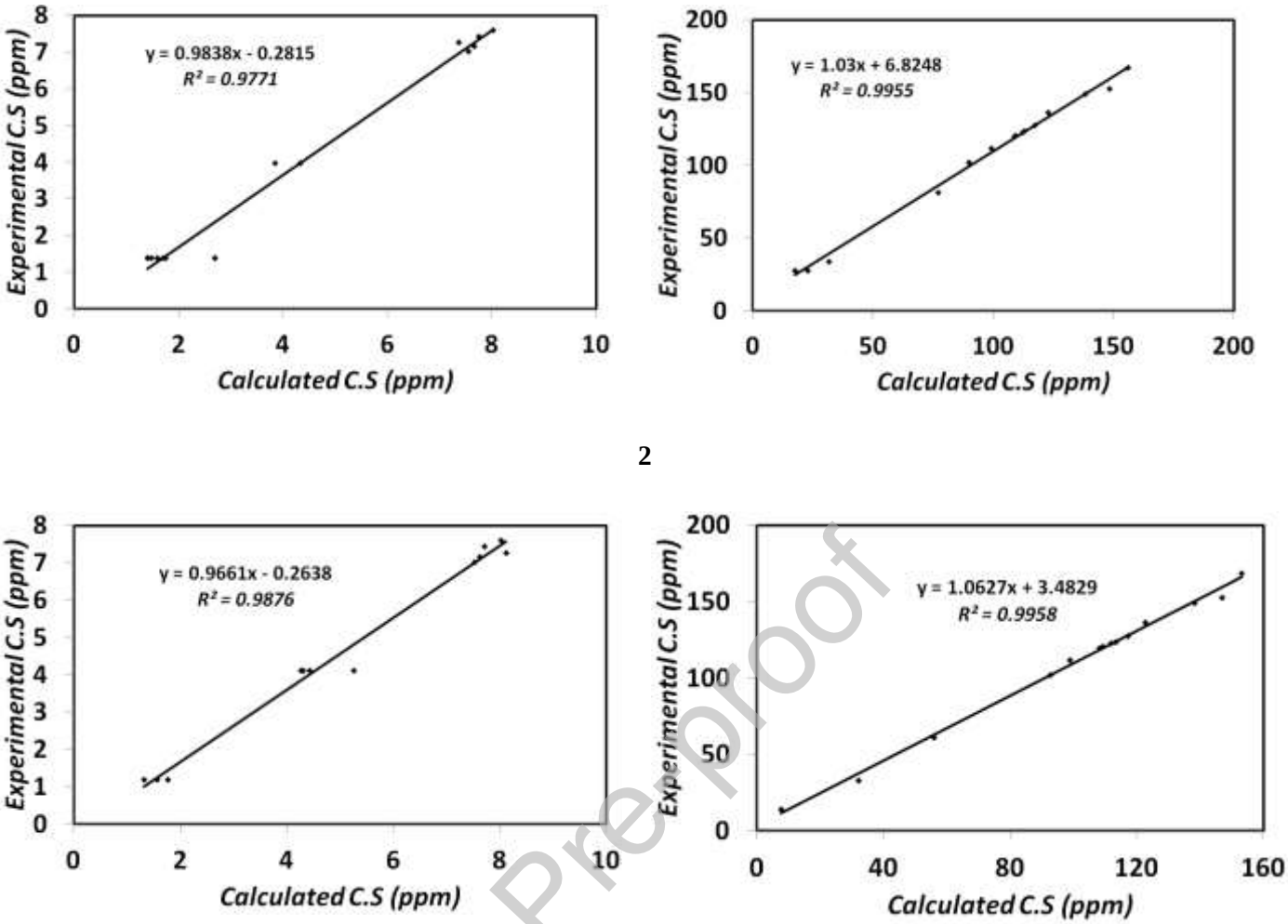

Fig. 16 Correlation graphs between the calculated and experimental ^{1}H and ^{13}C NMR chemical shifts. For protons chemical shifts, the chemical shifts of the NH protons were omitted from correlation graphs because the calculated chemical shifts of these labile protons deviated significantly from the experimental data. If considered, the correlation coefficients are 0.9155 and 0.8575 for **2** and **3**, respectively.

Conclusions

Two new hits of alkylsulfanyl-indolyltriazoles were synthesized *via* coupling of 4-amino-5-(1*H*-indol-2-yl)-1,2,4-triazol-3(2*H*)-thione **1** with two two halo esters in the presence of Et_3N. The alkylation were deduced to be done on sulfur using ^{13}C NMR signal around 34.00 ppm. The molecular architecture of the desired compounds were elucidated by the single crystal x-ray diffraction technique. The supramolecular structure of the studied compound is analyzed using Hirshfeld calculations. The different electron delocalization processes which stabilize

the studied systems were analyzed using NBO calculations. Also, the electronic and reactivity descriptors were also calculated and described. Finally concluded, the calculated NMR spectra are in good agreement with the experimental data.

Funding: The authors would like to extend their sincere appreciation to the Researchers Supporting project number (RSP-2020/64), King Saud University, Riyadh, Saudi Arabia.

Acknowledgments: The authors would like to extend their sincere appreciation to the Researchers Supporting project number (RSP-2020/64), King Saud University, Riyadh, Saudi Arabia.

Conflicts of Interest: The authors declare no conflict of interest.

author statement

Ahmed T. A. Boraei, Saied M. Soliman, Matti Haukka, and Assem Barakat: Conceptualization, Supervision: **Ahmed T. A. Boraei, and Assem Barakat**; Investigation, Methodology: **Ahmed T. A. Boraei, and Assem Barakat**; Data curation: **Saied M. Soliman and Matti Haukka**; Writing- Original draft preparation: **Ahmed T. A. Boraei, Saied M. Soliman, Matti Haukka, and Assem Barakat**; Software, Validation: **Saied M. Soliman**, and **Matti Haukka**; Writing- Reviewing and Editing, Approval the final manuscript: **All.**

References

[1] Mohammad, Y.; Fazili, K.M.; Bhat, K.A.; Ara, T. Synthesis and biological evaluation of novel 3-O-tethered triazoles of diosgenin as potent antiproliferative agents. *Steroids* **2017**, *118*, 1–8.

[2] Huang, M.; Deng, Z.; Tian, J.; Liu, T. Synthesis and biological evaluation of salinomycin triazole analogues as anticancer agents. *Eur. J. Med. Chem*. **2017**, *127*, 900–908.

[3] Gujjar, R.; Marwaha, A.; El Mazouni, F.; White, J.; White, K.L.; Creason, S.; Shackleford, D.M.; Baldwin, J.; Charman, W.N.; Buckner, F.S.; *et al*. Identification

of a metabolically stable triazolopyrimidine-based dihydroorotate dehydrogenase inhibitor with antimalarial activity in mice. *J. Med. Chem.*, **2009**, *52*, 1864–1872.

[4] Chen, M.; Lu, S.; Yuan, G.; Yang, S.; Du, X., Synthesis and antibacterial activity of some heterocyclic β-enamino ester derivatives with 1, 2, 3-triazole. *Heterocycl. Commun.* **2000**, *6*, 421–426.

[5] Ayati, A.; Emami, S.; Foroumadi, A. The importance of triazole scaffold in the development of anticonvulsant agents. *Eur. J. Med. Chem.* **2016**, *109*, 380–392.

[6] Akhtar, T.; Hameed, S.; Khan, K.M.; Choudhary, M.I., Syntheses, urease inhibition, and antimicrobial studies of some chiral 3-substituted-4-amino-5-thioxo-1*H*, 4*H*-1,2,4-triazoles. *Med. Chem.* **2008**, *4*, 539–543.

[7] Sevaille, L.; Gavara, L.; Bebrone, C.; De Luca, F.; Nauton, L.; Achard, M.; Mercuri, P.; Tanfoni, S.; Borgianni, L.; Guyon, C.; et al. 1,2,4-Triazole-3-thione compounds as inhibitors of dizinc metallo-β-lactamases. *ChemMedChem*, **2017**, *12*, 972–985.

[8] Gilmore, J.L.; King, B.W., Asakawa, N.; Harrison, K.; Tebben, A.; Sheppeck II, J.E.; Liu, R.Q.; Covington, M.; Duan, J.J.W. Synthesis and structure–activity relationship of a novel, non-hydroxamate series of TNF-α converting enzyme inhibitors. *Bioorg. Med. Chem. Lett.* **2007**, *17*, 4678–4682.

[9] Maingot, L.; Leroux, F.; Landry, V.; Dumont, J.; Nagase, H.; Villoutreix, B.; Sperandio, O.; Deprez-Poulain, R.; Deprez, B. New non-hydroxamic ADAMTS-5 inhibitors based on the 1,2,4-triazole-3-thiol scaffold. *Bioorg. Med. Chem. Lett.* **2010**, *20*, 6213–6216.

[10] Kruse, L.I.; Kaiser, C.; DeWolf, W.E.; Finkelstein, J.A.; Frazee, J.S.; Hilbert, E.L.; Ross, S.T.; Flaim, K.E.; Sawyer, J.L. Some benzyl-substituted imidazoles, triazoles, tetrazoles, pyridinethiones, and structural relatives as multisubstrate inhibitors of dopamine. *beta*.-hydroxylase. 4. Structure-activity relationships at the copper binding site. *J. Med. Chem.* **1990**, *33*, 781–789.

[11] Timur, İ.; Kocyigit, Ü.M.; Dastan, T.; Sandal, S.; Ceribası, A.O.; Taslimi, P.; Gulcin, İ.; Koparir, M.; Karatepe, M.; Çiftçi, M. In vitro cytotoxic and in vivo antitumoral activities of some aminomethyl derivatives of 2, 4-dihydro-3*H*-1,2,4-triazole-3-thiones—Evaluation of their acetylcholinesterase and carbonic anhydrase enzymes inhibition profiles. *J. Biochem. Mol. Toxic.* **2019,** *33*, e22239.

[12] Hamdy, R.; Ziedan, N.; Ali, S.; El-Sadek, M.; Lashin, E.; Brancale, A.; Jones, A.T.; Westwell, A.D. Synthesis and evaluation of 3-(benzylthio)-5-(1*H*-indol-3-yl)-

1,2,4-triazol-4-amines as Bcl-2 inhibitory anticancer agents. *Bioorg. Med. Chem. Lett.* **2013**, *23*, 2391–2394.

[13] Ziedan, N.I.; Hamdy, R.; Cavaliere, A.; Kourti, M.; Prencipe, F.; Brancale, A.; Jones, A.T.; Westwell, A.D. Virtual screening, SAR, and discovery of 5-(indole-3-yl)-2-[(2-nitrophenyl) amino][1,3,4]-oxadiazole as a novel Bcl-2 inhibitor. *Chem. Biol. Drug Des.* **2017**, *90*, 147–155.

[14] Boraei, A.T.; Ghabbour, H.A.; Gomaa, M.S.; El Ashry, E.S.H.; Barakat, A. Synthesis and anti-proliferative assessment of triazolo-thiadiazepine and triazolo-thiadiazine scaffolds. *Molecules* **2019,** *24*, p.4471.

[15] Boraei, A. T.; Singh, P. K.; Sechi, M..; Satta, S., Discovery of novel functionalized 1, 2, 4-triazoles as PARP-1 inhibitors in breast cancer: Design, synthesis and antitumor activity evaluation. *Eur. J. Med. Chem.* **2019,** *182*, 111621.

[16] Boraei, A.T.A.; Gomaa, M.S.; El Sayed, E.S.H.; Duerkop, A. Design, selective alkylation and X-ray crystal structure determination of dihydro-indolyl-1,2,4-triazole-3-thione and its 3-benzylsulfanyl analogue as potent anticancer agents. *Eur. J. Med. Chem.* **2017**, *125*, 360–371.

[17] Boraei, A. T.; Ashour, H. K.; El Sayed, H.; Abdelmoaty, N.; El-Falouji, A. I.; Gomaa, M. S., Design and synthesis of new phthalazine-based derivatives as potential EGFR inhibitors for the treatment of hepatocellular carcinoma. *Bioorg. Chem.* **2019**, *85*, 293–307.

[18] Darestani-Farahani, M.; Faridbod, F.; Ganjali, M.R., A sensitive fluorometric DNA nanobiosensor based on a new fluorophore for tumor suppressor gene detection. *Talanta* **2018**, *190*, 140–146.

[19] Shi, Z.; Zhao, Z.; Huang, M.; Fu, X. Ultrasound-assisted, one-pot, three-component synthesis and antibacterial activities of novel indole derivatives containing 1,3,4-oxadiazole and 1,2,4-triazole moieties. *C. R. Chim.* **2015**, *18*, 1320–1327.

[20] Baytaş, S.; Kapcak, E.; Çoban, T.; Özbilhe, H. Synthesis and antioxidant and antimicrobial evaluation of novel 4-substituted-1H-1, 2, 4-triazole derivatives. *Turk. J. Chem.*, **2012,** *36*(6), 867-884.

[21] Cascioferro, S.; Parrino, B.; Li Petri, G.; Cusumano, M.G.; Schillaci, D.; Sarno, V.D.; Musella, S.; Giovannetti, E.; Cirrincione, G.; Diana, P. 2,6-Disubstituted imidazo[2,1-*b*][1,3,4]thiadiazole derivatives as potent staphylococcal biofilm inhibitors. *Eur. J. Med. Chem.* **2019**, *167*, 200–210.

[22] Shi, Z.; Zhao, Z., Microwave irradiation synthesis of novel indole triazole Schiff base fluorescent probe for Al3+ ion. *Inorganica Chim. Acta* **2019**, *498*, 119135.

[23] Chehrouri, M.; Othman, A.A.; Jiménez-Cecilia, S.; Moreno-Cabrerizo, C.; Sansano, J.M.; 4-Amino-3-pentadecyl-3*H*-1,2,4-triazole-3-thiones and 3-pentadecyl-1,3,4-oxadiazole-2 (3*H*)-thione for the preparation of dimeric palladium (II) complexes and their applications in Tsuji–Trost and Mizoroki–Heck reactions. *Synth. Commun.* **2019**, *49*, 1301–1307.

[24] Ayoup, M. S.; Ahmed, H. E. A.; El Massry, A. M.; Senior, S.; Khattab, S. N.; Hassan, S. Y.; Amer, A. Synthesis, Docking, and Evaluation of Antimicrobial Activity of a New Series of Acyclo C-Nucleosides of 1,2,4-Triazolo [4,3-a] quinoxaline Derivatives. *J. Heterocycl. Chem.*, **2016**, *53*(1), 153-163.

[25] Amer, A.; Ayoup, M. S.; Khattab, S. N.; Hassan, S. Y.; Langer, V.; Senior, S.; El Massry, A. M. A regio-and stereo-controlled approach to triazoloquinoxalinyl C-nucleosides. *Carbohydr. Res.*, **2010**, *345*(17), 2474-2484.

[26] Boraei, A.T.A.; Sarhan, A.A.M.; Yousuf, S.; Barakat, A. Synthesis of a New Series of Nitrogen/Sulfur Heterocycles by Linking Four Rings: Indole; 1,2,4-Triazole; Pyridazine; and Quinoxaline. *Molecules* **2020**, *25*, 450.

[27] Sarhan, A.A.; Boraei, A.T.; Barakat, A.; Nafie, M.S. Discovery of hydrazide-based pyridazino [4, 5-b] indole scaffold as a new phosphoinositide 3-kinase (PI3K) inhibitor for breast cancer therapy. RSC Advances, **2020**, *10*(33), 19534-19541.

[28] Rikagu Oxford Diffraction, CrysAlisPro, Agilent Technologies inc., 2019, Yarnton, Oxfordshire, England.

[29] Sheldrick, G. M. Crystal structure refinement with SHELXL. *Acta Crystallogr. C*, **2015**, C71, 3-8.

[30] Hübschle, C. B.; Sheldrick, G. M.; Dittrich, B. ShelXle: a Qt graphical user interface for SHELXL. *J. Appl. Cryst.* **2011**, *44*, 1281-1284.

[31] Turner, M. J.; McKinnon, J. J.; Wolff, S. K.; Grimwood, D. J.; Spackman, P. R.; Jayatilaka, D.; Spackman, M. A. Crystal Explorer17 (2017) University of Western Australia. http://hirshfeldsurface.net

[32] a) Frisch, M.J.; Trucks, G.W.; Schlegel, H.B.; Scuseria, G.E.; Robb, M.A. et al., Gaussian, Inc., Wallingford CT, **2009,** 2009; b) GaussView, Version 4.1, R. Dennington II, T. Keith, J. Millam, Semichem Inc., Shawnee Mission, KS, (2007).

[33] Reed, A. E.; Curtiss, L. A.; Weinhold, F. Intermolecular interactions from a natural bond orbital, donor-acceptor viewpoint. *Chem. Rev.*, **1988**, *88*(6), 899–926.

[34] Marten, B.; Kim K.; Cortis, C.; Friesner, R. A.; Murphy, R. B.; Ringnalda, M. N.; Sitkoff, D.; Honig, B. New Model for Calculation of Solvation Free Energies: Correction of Self-Consistent Reaction Field Continuum Dielectric Theory for Short-Range Hydrogen-Bonding Effects, *J. Phys. Chem.* **1996,** *100*, 11775-11765.

[35] Tannor, D.J.; Marten, B.; Murphy, R.; Friesner, R.A.; Sitkoff, D.; Nicholls, A.; Ringnalda, M.; Goddard, W.A.; Honig, B. Accurate first principles calculation of molecular charge distributions and solvation energies from ab initio quantum mechanics and continuum dielectric theory. *J. Am. Chem. Soc.* **1994**, *116*, 11875–11882.

[36] Cheeseman, J.R.; Trucks, G.W.; Keith, T.A.; Frisch, M.J. A Comparison of Models for Calculating Nuclear Magnetic Resonance Shielding Tensors. *J. Chem. Phys.* **1996**, *104*, 5497–5509.

[37] Foresman, J.B.; Frisch, *Æ*. Exploring Chemistry with Electronic Structure Methods, second ed., Gaussian, Pittsburgh, PA, 1996.

[38] Chang, R. Chemistry, seventh ed., McGraw-Hill, New York, 2001.

[39] Kosar, B.; Albayrak, C. Spectroscopic investigations and quantum chemical computational study of (*E*)-4-methoxy-2-[(*p*-tolylimino) methyl] phenol. *Spectrochim. Acta A*, **2011**, *78*(1), 160-167.

[40] Koopmans, T. Ordering of wave functions and eigenenergies to the individual electrons of an atom. *Physica*, **1933**, *1*, 104-113.

[41] Parr, R.G.; W. Yang, Density-Functional Theory of Atoms and Molecules, Oxford University Press, New York, 1989.

[42] Parr, R. G.; Szentpaly, L. V.; Liu, S. Electrophilicity index. *J. Amer. Chem. Soc.*, **1999,** *121*(9), 1922-1924.

[43] Singh, R. N.; Kumar, A.; Tiwari, R. K.; Rawat, P.; Gupta, V. P. A combined experimental and quantum chemical (DFT and AIM) study on molecular structure, spectroscopic properties, NBO and multiple interaction analysis in a novel ethyl 4-[2-(carbamoyl) hydrazinylidene]-3, 5-dimethyl-1*H*-pyrrole-2-carboxylate and its dimer. *J. Mol. Struc.*, **2013**, *1035*, 427-440.

[44] Boraei, A.T.A.; Soliman, S.M.; Yousuf, S.; Barakat, A. Synthesis Single Crystal X-ray Structure DFT Studies and Hirshfeld Analysis of New Benzylsulfanyl-Triazolyl-Indole Scaffold. *Crystals* **2020**, *10*, 685.

[45] Joe, I. H.; Kostova, I.; Ravikumar, C.; Amalanathan, M.; Cîntă Pînzaru, S. Theoretical and vibrational spectral investigation of sodium salt of acenocoumarol. *J. Raman Spectrosc.*, **2009**, *40*(8), 1033-1038.

[46] Sebastian, S.; Sundaraganesan, N. The spectroscopic (FT-IR, FT-IR gas phase, FT-Raman and UV) and NBO analysis of 4-Hydroxypiperidine by density functional method. *Spectrochim. Acta A*, **2010,** *75*(3), 941-952.

GRAPHICAL ABSTRACT